PAPER

CrossMark
← click for updates

Orientation order and rotation mobility of nitroxide biradicals determined by quantitative simulation of EPR spectra†

Alexey V. Bogdanov* and Andrey Kh. Vorobiev

The problem of quantitative numerical simulation of electron paramagnetic resonance (EPR) spectra of biradical probes in both isotropic and aligned media was solved for the first time. The models suitable for the description of the spectra of the probes, both in the rigid limit and in the presence of rotational motions, were developed and successfully applied to model systems. The simulation of EPR spectra allows obtaining the following information about the molecular structure and dynamics: the values of orientation order parameters, the type of rotation mobility and its quantitative characteristics, and the sign and value of the spin exchange constant of the biradical. Model systems used in this work include solutions of nitroxide biradicals in a viscous solvent (squalane) in the range of temperatures 100–370 K and in the aligned liquid crystal n-octylcyanobiphenyl (8CB, 100–298.5 K). Unexpectedly, it was found that in 8CB the main orientation axis of the biradical molecule is perpendicular to the longest molecular axis.

I. Introduction

Electron paramagnetic resonance (EPR) is widely used to probe the structure and dynamics of soft materials: polymers,[1–4] glasses,[5,6] liquid crystals[7–10] and biological systems.[11–13] A particular advantage of EPR spectra is their profound dependence on the rotation mobility of paramagnetic species in the range of rotation correlation times of 10^{-6}–10^{-9} s and the orientation alignment of probe molecules in ordered environments.

For monoradicals it is generally agreed that the information about rotation mobility and orientation order should be extracted from EPR spectra *via* quantitative simulation of the spectra with the use of least-squares optimization. In order to obtain reliable results, the following criteria are proposed for the simulation procedure in the work of our group:[2,14]

(1) Discrepancies between the theoretical and experimental spectra should lie within the experimental errors.

(2) Optimization procedure should be stable with respect to the choice of the starting approximation within physically reasonable limits. It should be checked whether the spectral shape is sensitive to the change in the obtained parameters. Uncertainties and mutual dependencies of the model parameters should be considered.

(3) The resulting values of magnetic parameters, characteristics of rotation dynamics and orientation order parameters should be physically meaningful.

(4) For the given experimental system, simulation of a series of EPR spectra recorded at different temperatures, or at different sample orientations with respect to the magnetic field of the spectrometer, should give consistent and non-contradicting results.

In addition to points 1–4, multifrequency EPR studies proved to be useful to reveal the details of the spin probe motions, because spectra recorded at different frequencies may be sensitive to different aspects of molecular rotation mobility.[15]

For nitroxide monoradicals, extensively used as spin probes and spin labels, the problem of quantitative modeling of EPR spectra has been addressed and solved for many systems. Numerous models of spectral shape under various conditions have been proposed, and the standard software has been developed for spectral simulation.[14,16–18]

The use of spin probes containing two paramagnetic units in their structure (*i.e.*, biradicals) was suggested a long time ago,[19] however, there are few examples of such investigation. In most works, modulation of spin–spin interactions in flexible nitroxide biradicals due to their conformational changes was used to probe the conformational mobility and stiffness of liquid media.[20–22] The rotations of rigid biradicals were analyzed in the framework of Redfield's model, to account for EPR spectral linewidths in isotropic[23] and anisotropic[24] fluids.

The EPR spectra of nitroxide biradicals were simulated in the framework of stochastic Liouville equation (SLE) model in

Chemistry Department, Lomonosov Moscow State University, Leninskie gory, 1/3, Moscow, 119991, Russia. E-mail: avbgdn@gmail.com
† Electronic supplementary information (ESI) available. See DOI: 10.1039/c6cp05815a

the recent work of A. Polimeno *et al.*[25] For monoradical probes, this approach is widely used for the quantitative description of EPR spectra in the range of rotation correlation times $\tau_r = 10^{-6}$–10^{-10} s.[16] However, for biradicals, hitherto the SLE approach has only been tested for relatively fast rotations of probes in non-viscous isotropic solvents ($\tau_r = 10^{-9}$–10^{-10} s).[25]

In the present work, the use of the SLE approach is extended to the simulation of slow-motional EPR spectra of nitroxide biradicals. The other important application of spin probes in soft matter research is the determination of orientation alignment of molecules in partially ordered systems. In the present work we demonstrate the use of biradical spin probes for this purpose.

As model systems for the study, we employ the well-studied viscous solvent squalane in the range of temperatures 100–370 K and a liquid-crystalline solvent $4'$-*n*-octyl-4-cyanobiphenyl in the smectic phase (298.5 K) and in the supercooled smectic state at 100 K. We provide a quantitative simulation of EPR spectra of the nitroxide biradical in these solvents.

II. Experimental details

The structure of the used biradical is shown in Fig. 1. The material was synthesized according to the procedure described in ref. 26 and kindly provided by Prof. K. Hideg and Prof. A. I. Kokorin. Prior to use, the biradical was purified by thin-layer chromatography on Silufol plates. The concentration of the biradical in the samples was 10^{-4} mol L^{-1}.

Squalane (Aldrich) was stored over anhydrous NaOH. Before use, squalane was evacuated to 10^{-2} Torr to remove volatile impurities.

Liquid crystalline $4'$-octyl-4-cyanobiphenyl (8CB, Aldrich) was evacuated to 10^{-2} Torr prior to use, to remove volatile impurities. It exhibits two types of liquid-crystalline phases: the smectic A phase at 294–306 K and the nematic phase at 306–313 K.[27–29] To obtain an aligned liquid-crystalline material, the sample of 8CB doped with the biradical was slowly cooled in the magnetic field of an EPR spectrometer (about 3300 Gauss) from isotropic through nematic down to the smectic phase. This procedure gives the aligned liquid-crystalline sample. The aligned sample was quickly cooled in the spectrometer magnetic field to 100 K to obtain a supercooled smectic liquid crystal.

EPR spectra were recorded using an X-band spectrometer Bruker EMX plus. The temperature of the samples was set in the range 100–370 K using the flow of nitrogen gas. To compensate for systematic errors produced by the temperature control unit of the EPR spectrometer, the temperature of the

gas flow was calibrated using an external thermocouple. Thus, the accuracy of temperature setting was about ±0.5 K. For recording angular dependencies, the sample was rotated in the cavity of the EPR spectrometer using a goniometer setup. The accuracy of angle setting was ±0.2°.

III. Simulation of EPR spectra in the rigid limit

In this section we describe the procedure of simulation of EPR spectra of nitroxide biradicals in the absence of rotational motions of molecules (rigid limit). For each orientation of the biradical molecule, the EPR transition frequencies were calculated using the numerical solution of the following spin-Hamiltonian:

$$\frac{H}{g_0\mu_B} = \frac{H_0}{g_0}(\widetilde{\mathbf{n}}\overline{\overline{\mathbf{g}_1}}\mathbf{S}_1 + \widetilde{\mathbf{n}}\overline{\overline{\mathbf{g}_2}}\mathbf{S}_2) + \left(\widetilde{\mathbf{S}_1}\overline{\overline{\mathbf{A}_1}}\mathbf{I}_1 + \widetilde{\mathbf{S}_2}\overline{\overline{\mathbf{A}_2}}\mathbf{I}_2\right) + \widetilde{\mathbf{S}_1}\overline{\overline{\mathbf{D}}}\mathbf{S}_2 + J \cdot \widetilde{\mathbf{S}_1}\mathbf{S}_2 \tag{1}$$

where H is the spin-Hamiltonian operator; g_0 is the average g-factor of the paramagnetic moiety $\left(g_0 = \sqrt{\mathrm{Tr}(\widetilde{\mathbf{g}_1}\mathbf{g}_1)/3}\right)$; μ_B is the Bohr magneton; H_0 is the flux density of the magnetic field of an EPR spectrometer; $\mathbf{n}$ is the unit vector of magnetic field direction; $\tilde{\mathbf{n}} = (0,0,1)$, $\mathbf{S}_k = (S_{xk}, S_{yk}, S_{zk})$ and $\mathbf{I}_k = (I_{xk}, I_{yk}, I_{zk})$ are electron and nuclear spin operators for each of the two paramagnetic centers of the biradical molecule ($k = 1, 2$); $\overline{\overline{\mathbf{g}_k}}$, $\overline{\overline{\mathbf{D}}}$, and $\overline{\overline{\mathbf{A}_k}}$ are tensors of Zeeman, dipolar and hyperfine interactions; J is the spin exchange constant; and tilde denotes vector or matrix transposition.

Hyperfine interaction was calculated within the high-field approximation:[30,31]

$$\widetilde{\mathbf{S}_k}\overline{\overline{\mathbf{A}_k}}\mathbf{I}_k \approx A_{\mathrm{eff},k}S_{z,k}m_{z,k} \tag{2}$$

where $m_{z,k}$ is the projection of the nuclear spin and $A_{\mathrm{eff},k} = \frac{\sqrt{\widetilde{\mathbf{n}}\mathbf{g}_k\mathbf{A}_k\widetilde{\mathbf{A}_k}\widetilde{\mathbf{g}_k}\mathbf{n}}}{\sqrt{\mathrm{Tr}(\widetilde{\mathbf{g}_k}\mathbf{g}_k)/3}}$ is the effective value of the hyperfine interaction tensor. The spin-Hamiltonian was represented in the basis of electron spin operators $\mathbf{S}_1 \otimes \mathbf{S}_2$, thus, as a 4×4 matrix. The analytical expressions for the eigenvalues of this matrix can be obtained only for coaxial magnetic tensors.[32] In this work, the spin-Hamiltonian was diagonalised numerically, in the general form.

The dipolar tensor was calculated within the point dipole approximation:

$$\overline{\overline{\mathbf{D}}} = \frac{\mu_0}{4\pi}\frac{\mu_B^2 g_e^2}{r^5}\begin{pmatrix} r^2 - 3x^2 & -3xy & -3xz \\ -3xy & r^2 - 3y^2 & -3yz \\ -3xz & -3yz & r^2 - 3z^2 \end{pmatrix}$$
$$= \frac{18\,561\ \mathrm{Gauss}^3}{r^5} \cdot \begin{pmatrix} r^2 - 3x^2 & -3xy & -3xz \\ -3xy & r^2 - 3y^2 & -3yz \\ -3xz & -3yz & r^2 - 3z^2 \end{pmatrix} \tag{3}$$
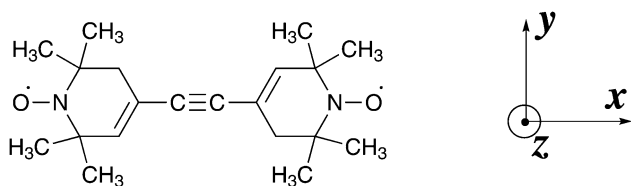
Fig. 1 The structure of the biradical used in the present work and a schematic illustration of molecular axes.

where $\frac{\mu_0}{4\pi} = 10^{-7}\frac{N}{A^2}$ is the magnetic constant and $\mathbf{r} = (x,y,z)$ is the radius-vector connecting two paramagnetic centers, $r^2 = x^2 + y^2 + z^2$.

The transition probabilities were calculated using the perturbation theory, with the following perturbation Hamiltonian:

$$H_1 = \mu_B H_1 \big(\widetilde{\mathbf{n}}_1 \overline{\overline{\mathbf{g}_1}} \mathbf{S}_1 + \widetilde{\mathbf{n}}_1 \overline{\overline{\mathbf{g}_2}} \mathbf{S}_2 \big) \qquad (4)$$

where H_1 is the flux density of the microwave magnetic field. The direction of the flux density of the microwave magnetic field was supposed to coincide with the y-axis of the laboratory reference frame: $\tilde{\mathbf{n}}_1 = (0,1,0)$. The transition intensities P_{ij} are proportional to squares of matrix elements of $\tilde{\mathbf{V}} H_1 \mathbf{V}$, where the columns of matrix $\mathbf{V}$ correspond to eigenvectors of unperturbed spin-Hamiltonian H:

$$P_{ij} \sim |(\tilde{\mathbf{V}} H_1 \mathbf{V})_{ij}|^2. \qquad (5)$$

There are 54 non-degenerate transitions, 18 of which correspond to simultaneous spin flips of both electrons, and are forbidden.

Thus, for each orientation of biradicals in the magnetic field of an EPR spectrometer, the spectral shape can be described by a function $f(B,\Omega_{LM})$, which is a superposition of individual spectral lines, corresponding to eigenvalues of the spin-Hamiltonian (1), with intensities, given by (5). The line positions and intensities depend on the molecule orientation, $i.e.$ on the Euler angles $\Omega_{LM} = (\varphi, \theta, \psi)$, which transform the laboratory reference frame into the molecular frame. The individual line was described by the Voigt profile, which is the envelope of Gaussian and Lorentzian profiles.[33] The Gaussian and Lorentzian linewidths were assumed to be dependent on the molecule orientation, and treated as tensors of rank two.[14] The EPR spectrum of the sample, which contains biradicals in different orientations, is given by:

$$I(B) = \int f(B,\Omega_{LM})\rho(\Omega_{LM})\mathrm{d}\Omega_{LM} \qquad (6)$$

where $\mathrm{d}\Omega_{LM} = \sin\theta \cdot \mathrm{d}\varphi \mathrm{d}\theta \mathrm{d}\psi$, $\rho(\Omega_{LM})$ is the number density of particles with orientation Ω_{LM}. The function $\rho(\Omega_{LM})$ is called the orientation distribution function.[34] It is represented as a series of Wigner D-functions:

$$\rho(\Omega_{LM}) = \sum_{j=0}^{\infty}\sum_{m=-j}^{j}\sum_{n=-j}^{j}\frac{2j+1}{8\pi^2}\langle \mathbf{D}_{mn}^{*j}\rangle \mathbf{D}_{mn}^{j}(\Omega_{LM}) \qquad (7)$$

where the values $\langle \mathbf{D}_{mn}^{*j}\rangle$ compose the set of order parameters. For practical calculations, the series in (7) is truncated at $j = J_{max}$, chosen so that the further increase of J_{max} does not lead to a change in the spectral shape.

To sum up, the spectrum of nitroxide biradicals in rigid limit was calculated using eqn (6), with the orientation distribution function defined by eqn (7) and the spectral function for individual orientation $f(B,\Omega_{LM})$ determined from the spin-Hamiltonian (1).

IV. Simulation of EPR spectra of rotating biradicals

In the slow-motional regime, the stochastic Liouville equation approach was used for the simulation of the spectra. According to this approach, the frequency-swept EPR spectrum in the absence of saturation is given by the equation:[16,35]

$$I(\omega - \omega_0) = \left(\frac{1}{\pi}\right)\left\langle v \left| \left[\left(\widetilde{\mathbf{\Gamma}} - i\mathbf{L}\right) + i(\omega - \omega_0)\mathbf{E}\right]^{-1} \right| v\right\rangle \qquad (8)$$

where ω is the microwave frequency, $\omega_0 = g_0\mu_B B_0/\hbar$, $\left(\widetilde{\mathbf{\Gamma}} - i\mathbf{L}\right)$ is the stochastic Liouville superoperator,[36,37] $\mathbf{E}$ is the identity operator, and v is the starting vector, which defines the spin operator for EPR transitions and the orientation distribution function for oriented systems.

The Liouville superoperator depends on spatial (orientation) coordinates and spin coordinates. The generally accepted basis for the orientation part consists of orthonormalised Wigner functions:[15,16,38]

$$|L, M, K\rangle = \sqrt{\frac{2L+1}{8\pi^2}}\mathbf{D}_{MK}^{L}(\Omega) \qquad (9)$$

where Ω is a set of Euler angles, which transform the laboratory frame into the molecular frame. The spin part of the Liouville superoperator is represented in the basis of spin transitions denoted as $|p_1^S, q_1^S, p_2^S, q_2^S\rangle \otimes |p_1^I, q_1^I, p_2^I, q_2^I\rangle$. For the transition between states with spin quantum numbers $m_{S,i}$ and $m_{S,i}{}'$ ($i = 1, 2$ is the number of paramagnetic centers in a biradical), the quantities p_i^S and q_i^S are defined as $p_i^S = m_{S,i} - m_{S,i}{}'$, $q_i^S = m_{S,i} - m_{S,i}{}'$, similarly to nuclear spin states p_i^I and q_i^I.

A nitroxide biradical has 36 possible spin states, with $36 \times 35/2 = 630$ possible spin transitions between them, which lead to very large dimensions of basis sets needed for the simulation of slow-motional EPR spectra. The following selection rules can greatly reduce the dimension of the basis:

– for EPR spectral simulation, only transitions with $|p_1^S, q_1^S, p_2^S, q_2^S\rangle = |0,-1,1,0\rangle$, $|0,1,1,0\rangle$, $|1,0,0,-1\rangle$, $|1,0,0,1\rangle$ need to be considered, which corresponds to the change in the spin state of only one paramagnetic center;

– for isotropic systems, only basis vectors with $p_I^1 + p_I^2 = M$ have non-zero matrix elements for the Liouville superoperator, similarly to the case of monoradicals. The same holds for ordered samples, in the case when the sample director coincides with the spectrometer magnetic field.[38] For spectra recorded at the sample director tilted with respect to the spectrometer magnetic field, this condition is no longer applicable, which leads to enormous basis set sizes. In this situation, the basis set was diminished by the pruning procedure, described in detail in ref. 39.

A further reduction of the basis set with respect to spatial coordinates can be achieved by applying symmetry arguments in ref. 38 (p. 3935).

The operator $\widetilde{\mathbf{\Gamma}}$ in (8) describes the relaxation of the system. In this work, the orientation relaxation of the spin probes was treated in the framework of the rotation diffusion model.[38,40]

For the description of rotation and orientation of the spin probes in the aligned liquid crystal, the mean-field potential model[36,38] was used. According to this model, the probe undergoes rotation diffusion in the orientation-dependent potential $U(\Omega)$, which averages the forces imposed by the surrounding liquid crystal molecules. The potential was represented as a series in Wigner functions:

$$U(\Omega) = k_B T \cdot \sum_{j=0}^{\infty} \sum_{n=-j}^{j} c_n^j \mathbf{D}_{0n}^j(\Omega). \tag{10}$$

The potential was considered macroscopically axial and microscopically orthorhombic, as in ref. 15, 38, and 40, which implies for the expansion coefficients in (10) that $c_n^j = c_{-n}^j$ and all c_n^j are real. The orientation order parameters, corresponding to the potential $U(\Omega)$, are given by

$$\langle \mathbf{D}_{mn}^{*j} \rangle = \frac{\int \mathbf{D}_{mn}^{*j}(\Omega) e^{-U(\Omega)/k_B T} d\Omega}{\int e^{-U(\Omega)/k_B T} d\Omega}. \tag{11}$$

Due to the above-mentioned symmetry properties of the potential, only order parameters $\langle \mathbf{D}_{0n}^{*j} \rangle$ with even n are non-zero.

For the interpretation of EPR spectra obtained in the present work, the model of rotation diffusion in the mean-field potential was generalised for the case of arbitrary orientation of the rotation diffusion tensor with respect to the mean-field potential reference frame, *i.e.* the case when the principal axes of rotation and orientation do not coincide. The derivation of expressions for matrix elements of the Liouville superoperator for this case is presented in the ESI.† The example and physical meaning of this situation will be discussed in Section VII.

Sometimes it is suggested to apply the SLE approach to the simulation of rigid limit spectra, by setting rotation diffusion coefficients smaller than $\sim 10^6$ s^{-1}. However, this approach demands using impractically large basis sets,[16] and does not allow for independent determination of orientation order parameters in the case of ordered samples.[41] For these reasons, in this work, the rigid limit spectra are described in the framework of the model described in Section III, whereas the SLE approach was applied to the spectra in the slow-motional regime.

V. Details of optimization procedure

To extract information from experimental EPR spectra, the numerical modeling of the spectra with the use of a nonlinear least-squares technique was performed. This procedure involves the minimization of the sum of squared deviations of the theoretical spectra from the experimental ones. The minimization was performed using the adaptive algorithm.[42]

The errors of the varied values can be estimated by evaluating the diagonal elements of the Hessian matrix in the optimum point.[42] However, this procedure allows considering only statistical errors of the optimization procedure and tends to underestimate the error values.

In the cases when the interpretation of results called for more accurate estimation of uncertainties, the following procedure was used. For the given varied parameter x, the parameter was shifted from the optimum value x_0 by a small step Δx. Thus, the value of this parameter was fixed at $x_0 \pm \Delta x$, and all other varied parameters were re-optimised to obtain the conditional minimum. The value of the objective function (*i.e.* the sum of squared deviations of the theoretical spectrum from the experimental one, related to the number of points in the spectrum), corresponding to the new parameter value $x_0 \pm \Delta x$ increased by the value $\Delta f_\pm$ with respect to the optimum value. This increase can be compared with the intrinsic experimental noise of the spectrum Δ_c, which was measured as the variance of the baseline of the experimental spectrum. Then, by assuming quadratic dependence of the objective function on the parameter in the vicinity of minimum, one can estimate the error $\varepsilon_{x,\pm}$ of parameter x as the deviation Δx, which corresponds to the increase of the objective function as large as the value of experimental noise:

$$\varepsilon_{x,\pm} = \sqrt{\frac{\Delta_c}{\Delta f_\pm}} \cdot \Delta x. \tag{12}$$

This procedure implicitly accounts for errors connected with the mutual dependence of model parameters. In the present work it was applied for evaluating the uncertainties of the spin exchange constant J and all Euler angles.

VI. EPR spectra of the biradical in squalane

The experimentally recorded spectra of the biradical in squalane over the range of temperatures 100–370 K are shown in Fig. 2 as black lines. The theoretical spectra obtained as a result of simulation are presented as red lines. A quantitative agreement between the experimental spectra and theoretical ones was achieved.

It was found that the EPR spectra are complicated by the presence of monoradical impurity. This can be well seen in the spectrum recorded at 271 K (Fig. 2): a clearly observed sharp line in the low field (marked by blue arrow) is related to the monoradical admixture. Even at very low content of monoradicals, they can considerably contribute to the spectral shape, because of the following reasons:

– the intensity of monoradical spectra is divided only between three lines, whereas in the case of biradicals, there are generally more lines;

– monoradical lines are often narrower than those of biradical lines; this may be due to the large anisotropic dipolar interaction, which is not completely averaged given that the biradical rotation is not sufficiently fast.

Due to these reasons, one of the prerequisites for working with biradicals as spin probes is the thorough purification of the used materials, including solvents. Thus, it is known[43] that in the presence of Lewis acids, the disproportionation reaction between two nitroxyl radicals in solution takes place, to form hydroxylamine and the nitrosonium cation. In the case of monoradicals, this reaction only decreases the EPR signal intensity slightly, without changing the spectral shape. In the case of biradicals, bimolecular disproportionation leads to the transformation of two biradical molecules into monoradicals,
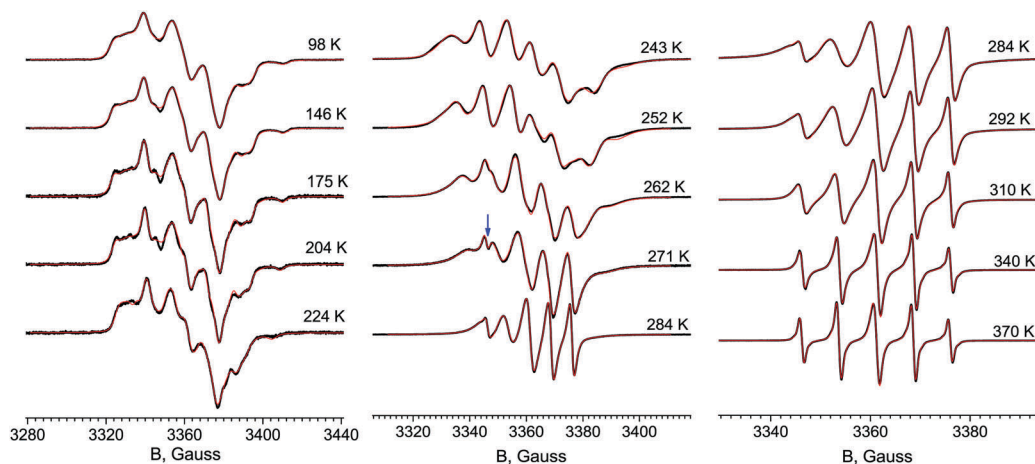
Fig. 2 EPR spectra of the studied biradical in squalane at 98–370 K (black lines: experiment, red lines: simulation).

which results in the essential change in the EPR spectral shape. For this reason, acidic impurities, including water, should be avoided when working with biradical probes. For the same reason, the solvents must be thoroughly purified to eliminate reactive impurities, such as peroxides.

The numerical simulation of spectra in Fig. 2 shows that the contribution of the monoradical admixture to the double integral of EPR spectra is 0.8%. Even at such a low concentration, for quantitative simulation of the spectra, the monoradical impurity should be explicitly included in the model, for both low- and high-temperature spectra. In the present work, the EPR spectra were calculated as superposition of the biradical spectrum and the monoradical spectrum. For the simulation of the monoradical spectrum, the same principal values of Zeeman and hyperfine interaction tensors as observed for the biradical were used.

At low temperatures, below the glass transition point of squalane ($T < 200$ K), EPR spectra are successfully simulated in the model of rigid limit. In the vicinity of the glass transition point (200–230 K), the spectra retain the shape characteristic of rigid limit, however, the apparent principal values of magnetic tensors determined in the course of spectral simulation are different from those at low temperatures. Partial averaging of magnetic tensors is observed. For monoradicals,[5,14,44,45] such behaviour is known to originate from quasi-libration motions of the probes, *i.e.* fast stochastic reorientations of the probe molecule within the solvent cage with limited amplitudes.

It was found that EPR spectra of the biradical investigated in the present work at these temperatures can be successfully simulated in the framework of the quasi-libration model. It was discovered that taking into account quasi-librations just around the *x*-axis of the biradical molecule (see Fig. 1 for designations of axes) is sufficient to quantitatively simulate EPR spectra. The tensor averaging in this case is expressed by the equation:

$$\mathbf{g}_L = \frac{1}{2L_X} \int_{-L_X}^{+L_X} d\psi\, \mathbf{R}(\psi)\mathbf{g}_0 \mathbf{R}^{\mathrm{T}}(\psi) \qquad (13)$$

where $\mathbf{g}_L$ is the apparent **g**-tensor in the presence of libration motions, $\mathbf{g}_0$ is the initial **g**-tensor in the absence of rotational motions, L_X is the quasi-libration half-amplitude, and $\mathbf{R}(\psi)$ is the rotation matrix for rotation by angle ψ around the *x*-axis. Expressions analogous to (13) hold for the averaging of hyperfine interaction and dipolar interaction tensors.

For the determination of quasi-libration amplitudes from the experimental spectra in the course of spectral simulation, the principal values of the magnetic parameters were taken equal to those determined from the lowest-temperature spectrum (98 K) and were not varied. These values are listed in Table 1. The other parameters (*i.e.*, linewidths and quasi-libration amplitudes) were varied to obtain the optimum description of the experimental spectrum. The quasi-libration amplitudes determined in the course of this procedure are shown in Fig. 3.

At temperatures higher than 230 K, the EPR spectral shape changes significantly. These changes indicate the transition to the slow-motional regime. In this regime, the spectra were simulated with the use of the stochastic Liouville equation.

As shown in ref. 46, in the geometrical structure of the biradical, the fragment C=C–C≡C–C=C is planar, but due to the twist of the piperidine rings, the magnetic tensors of the two nitroxides are tilted by a small angle θ (*cf.* Table 1) around the axis of NO-bonds. Thus, the molecule of the investigated biradical is characterized by symmetry group C_2, with three 2-fold symmetry axes, one of which is directed along the *x*-axis of magnetic tensors, and two others make an angle $\theta/2 \approx 7.9°$ with *y*- and *z*-axes of magnetic tensors. It would be natural to

Table 1 Magnetic parameters of the biradical molecule determined from the lowest temperature spectrum (98 K). $g_{\alpha\alpha}$ and $A_{\alpha\alpha}$ ($\alpha = x, y, z$) are principal values of Zeeman and hyperfine interaction tensors; *x*, *y*, and *z* are components of the dipolar vector (*cf.* eqn (3)), θ is the angle between the principal *z*-axes of **g**-tensors of the two paramagnetic centers. **g**- and **A**-tensors of the same paramagnetic center are assumed to be coaxial

g_{xx} 2.00936 ± 0.00010	A_{xx}, Gauss 5.2 ± 0.5	x, Å 10.66 ± 0.02
g_{yy} 2.00656 ± 0.00010	A_{yy}, Gauss 7.3 ± 0.3	$y = z = 0$
g_{zz} 2.00238 ± 0.00010	A_{zz}, Gauss 32.09 ± 0.11	θ, ° 15.7 ± 0.6
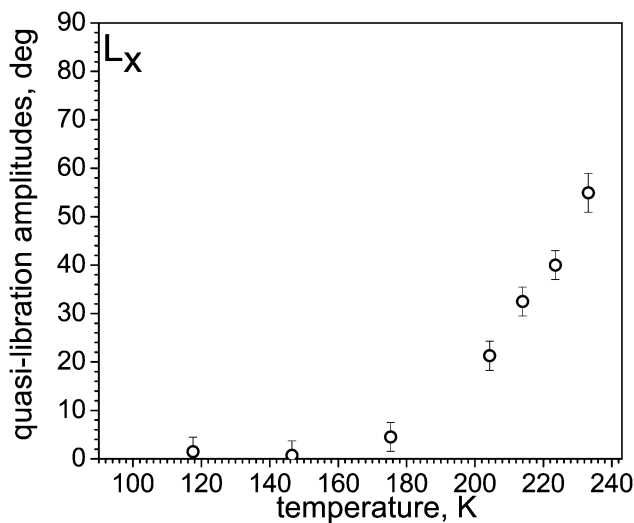
Fig. 3 Quasi-libration half-amplitudes around the *x*-axis of the probe molecule.

Fig. 4 Principal values of the rotation diffusion tensor of the biradical in squalane.

expect the principal axes of the rotation diffusion tensor to be directed along the symmetry axes of the probe molecule. However, it should be taken into account that the probe molecule can exist in two mutually enantiomeric conformers, corresponding to different directions of the twist between piperidine rings (+θ and −θ). The energy barrier between these conformers was estimated in ref. 46 to be about 4 kJ mol⁻¹ from quantum-chemical calculations *in vacuo*, and estimated in this work to be about 16 kJ mol⁻¹ in squalane (see below). Therefore, at higher temperatures in the investigated temperature range the fast interconversion between the two conformers may take place. This interconversion leads to the averaging of magnetic tensors according to the equation:

$$\langle g_{xx}\rangle = g_{xx}$$
$$\langle g_{yy}\rangle = g_{yy}\cos^2\theta + g_{zz}\sin^2\theta \quad (14)$$
$$\langle g_{yy}\rangle = g_{yy}\sin^2\theta + g_{zz}\cos^2\theta$$

where angular brackets denote the averaged values of the **g**-tensor, and the analogous equation holds for the averaging of the hyperfine interaction tensor.

It has been found that the two approaches explained above: with and without accounting for the fast conformational mobility of the biradical, lead to an almost identical description of experimental spectra, and result in very close values of rotation diffusion coefficients.

The principal values of the rotation diffusion tensor are presented in Fig. 4. At temperatures 250–280 K, the values of the rotation diffusion coefficient around the molecular *z*-axis are determined with large errors. EPR spectra can be simulated equally well using the values of R_z in a very wide range (Fig. 4).

At temperatures higher than 284 K the rotation diffusion tensor is apparently axial, *i.e.* the rotations around *y*- and *z*-axes of the biradical are characterized by the same value of the rotation diffusion coefficient. The reason for this may be the
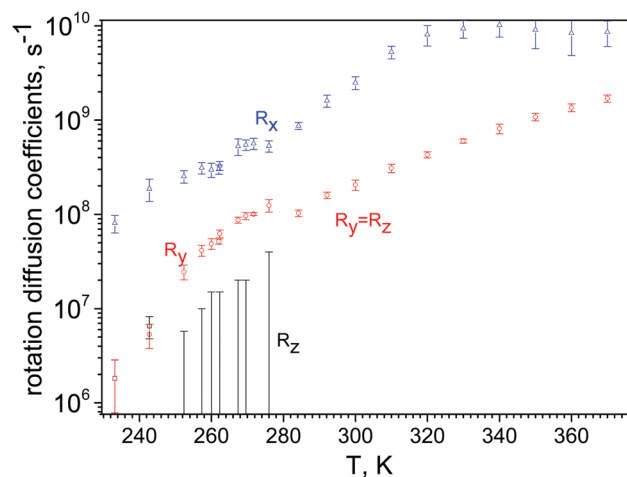
enhancement of conformational mobility of the biradical: when the mutual rotation of the two piperidine rings takes place as fast as the rotation of the probe molecule as a whole, the axes perpendicular to the principal rotation axis are no longer discerned. Given the temperature at which this occurs (≈284 K), one may roughly estimate the energy barrier of the internal rotation E_{rot}. Using Eyring's equation,[47] we may estimate the characteristic time of internal rotation τ_{int}:

$$\frac{1}{\tau_{int}} = \frac{k_B T}{h}\exp\left(-\frac{E_{rot}}{RT}\right). \quad (15)$$

On the other hand, the correlation time of rotation around the *x*-axis of the molecule as a whole, $\tau_{rot,x}$, is inversely proportional to the corresponding rotation diffusion coefficient:

$$\frac{1}{\tau_{rot,x}} = 6R_x. \quad (16)$$

By substituting T = 284 K and R_x = 8.7 × 10⁸ s⁻¹ (see Fig. 4) into eqn (15) and (16), we find that the condition $\tau_{rot,x} \sim \tau_{int}$ is fulfilled at $E_{rot} \sim 16$ kJ mol⁻¹. The quantum chemical calculation gives the estimate of $E_{rot} \approx 4$ kJ mol⁻¹.[46] Taking into account that quantum chemical calculations were performed *in vacuo*, these values are not in contradiction.

Fig. 4 demonstrates that the EPR spectra of biradicals are sensitive to the molecular rotational movements with the diffusion coefficients mostly in the range 10⁷–10¹⁰ s⁻¹.

The simulation of EPR spectra also provides some information about the value and the absolute sign of the spin exchange constant (J in eqn (1)). It is known[48] that the EPR spectra of biradicals both in the rigid limit and in the limit of fast rotations are only dependent on the absolute value of J. However, in the slow-motional regime, due to non-complete averaging of anisotropic interactions, the shape of the EPR spectra depends on the sign of the spin exchange constant.[25] This is illustrated in Fig. 5a. It demonstrates the experimental EPR spectrum recorded at 320 K and the best-fit theoretical spectra in the assumption of positive and negative signs of J. It has been
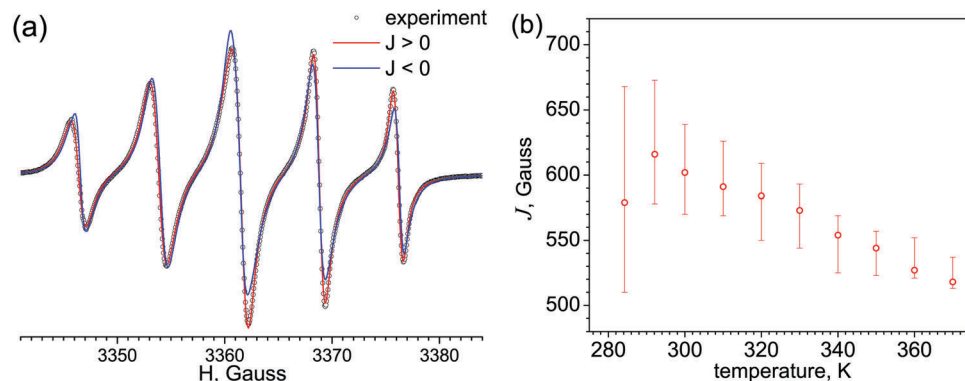
Fig. 5 (a) The best-fit simulation of the EPR spectrum of the biradical recorded at 320 K, with positive (red line) and negative (blue line) spin exchange constants J. The experimental spectrum is shown as black points. (b) Temperature dependence of the spin exchange constant J determined from EPR spectral simulation.

found that the positive sign of J ($J > 0$) gives better description of experimental EPR spectra at all temperatures in the slow-motional regime of biradical rotations. This means that the singlet level of the investigated biradical lies below the triplet level.

It has been found that the accuracy of the absolute values of the spin exchange constant determined from the EPR spectra largely depends on the shape of the spectra. This is due to the fact that for the investigated biradical the spin exchange constant is much higher than the hyperfine splitting constant, $J \gg a$. In this condition, the positions of EPR lines are only slightly dependent on the value of J,[25,48] and the accurate determination of J is only possible if the spectra are sufficiently narrow. For example, at 175 K the EPR spectrum is broad, and the value of J is determined to be $J = 610^{+440}_{-240}$ Gauss.

At temperatures above $\sim$280 K, EPR spectra become narrower and allow for more accurate determination of the spin exchange constant. The values of J obtained at temperatures $T > 280$ K are shown in Fig. 5b. It is seen that in this temperature range the slight decrease of the spin exchange constant with temperature is observed. This decrease is readily explained by the conformational mobility of the biradical. The value of the spin exchange is determined by the overlap of spin-orbitals containing unpaired electrons of the biradical. This overlap depends on the conjugation in the π-system of the biradical molecule (see Fig. 1). It is largest when the two piperidine rings are parallel, and is close to zero if they are orthogonal. The mutual rotation of nitroxide moieties should lead to a decrease of the spin-orbital overlap, and therefore to the decrease of the spin exchange constant, which is indeed observed experimentally with the increase of temperature.

Thus, the experiment indicates that the internal rotation is sufficiently fast to average spin exchange constant over the rotamers. On the other hand, the rates of internal rotation can be estimated on the basis of the rotation diffusion constant around the biradical x-axis, which is plotted against temperature in Fig. 4. For example, at 284 K the estimate of the characteristic rotation time is $\tau \sim 1/(6R_x) \approx 2 \times 10^{-10}$ s. As it has been shown previously,[21] this time corresponds to the transition to the fast-motion regime, where the spin exchange constant effectively averages over possible conformers. Therefore, this estimate is in agreement with the fact that at temperatures higher than 284 K, the EPR spectra are well described by averaged values of J. At lower temperatures, as it has been stated above, the spin exchange constant is determined with high uncertainty, due to the large spectral linewidth. Under these conditions, the possible changes in the spectra shape related to the spin exchange constant modulation due to slow internal rotation may be masked by the large linewidths.

VII. EPR spectra of the biradical in 8CB

The aligned samples of the biradical in liquid crystalline 4′-octyl-4-cyanobiphenyl (8CB) were prepared as described in Section II. For the ordered samples, the angular dependence of the EPR spectrum of the biradical, *i.e.* the dependence of the spectrum on the angle between the sample director and the magnetic field of the EPR spectrometer, was recorded. The angular dependencies were recorded in the smectic phase of 8CB (Fig. 6a) and in the supercooled smectic state at 100 K (Fig. 6b).

The magnetic parameters used for numerical simulation of angular dependencies were the same as those determined from the EPR spectra of the biradical in squalane at 98 K (listed in Table 1). The value of spin exchange constant J was varied in the course of the simulation, and for both angular dependencies it was found to be (700 ± 100) Gauss.

For modeling of the spectra in the supercooled smectic state, the rigid limit approach was used (see Section III). The values of orientation order parameters $\left\langle \mathbf{D}^{j*}_{m,n} \right\rangle$ were varied to obtain the best fit. It was found that the truncation of the series (7) to $J_{\max} = 6$ is sufficient for the spectral simulation, and the further increase of $J_{\max}$ does not lead to the change in the theoretical spectra. As in Section VI, the monoradical additive was explicitly included in the simulation. Due to the small amount of monoradical impurity, the orientation order parameters of the monoradical cannot be separately determined
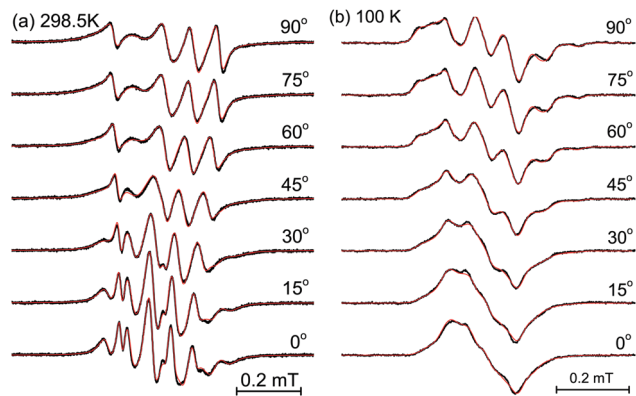
Fig. 6 Angular dependency of EPR spectra of the studied biradical in 8CB at 298.5 K (a) and 100 K (b).

Table 2 The values of orientation and rotation characteristics of the biradical in 8CB, determined from the result of numerical simulation of angular dependencies of EPR spectra recorded in the smectic (298.5 K) and supercooled smectic (100 K) states

Parameter		298.5 K	100 K
$\langle \mathbf{D}_{0,0}^{2*} \rangle$		0.372	0.537 ± 0.006
$\langle \mathbf{D}_{0,0}^{4*} \rangle$		0.144	0.169 ± 0.008
$\langle \mathbf{D}_{0,0}^{6*} \rangle$		0.044	0.033 ± 0.008
$\langle \mathbf{D}_{0,2}^{2*} \rangle$		-0.017	0
Mean-field potential decomposition coefficients c_n^j		$c_0^2 = 1.49$ $c_2^2 = -0.17$ $c_0^4 = 0.41$	—
$\Omega_{g\to ori}$, degrees	α	111 ± 3	89 ± 30
	β	103 ± 8	115 ± 10
	γ	95 ± 7	—
R_x, s^{-1}		$(2.1 \pm 0.4) \times 10^7$	—
R_y, s^{-1}		$(7.3 \pm 0.4) \times 10^7$	—
R_z, s^{-1}		$(4.8 \pm 0.2) \times 10^8$	—
$\Omega_{\text{Diff}\to ori}$, degrees	α	46 ± 23	—
	β	85 ± 10	—
	γ	0	—

from the spectra. These order parameters were fixed equal to the corresponding values of the biradical.

For modeling of the angular dependence of EPR spectra in the smectic state, the stochastic Liouville equation approach was applied (see Section IV). In this case, the varied parameters were the principal values of the rotation diffusion tensor and the expansion coefficients c_n^j of the mean-field potential (eqn (10)). Only three coefficients c_0^2, c_2^2 and c_0^4 were found to be sufficient for simulation. It has been found that taking into account the conformational mobility of the biradical according to eqn (14) gives somewhat better description of experimental spectra.

The best-fit theoretical spectra obtained in the course of simulation are presented in Fig. 6 as red lines. The quantitative agreement between the experimental spectra and the theoretical ones is observed, both in the smectic and supercooled smectic states. It is important to note that the same set of magnetic parameters was used for the simulation of the spectra of the biradical in squalane and in aligned samples of 8CB. To our knowledge, this is the first example of quantitative numerical simulation of angular dependencies of EPR spectra for biradical probes.

The values of orientation order parameters determined from the results of simulation are presented in Table 2. For spectra recorded at 100 K, order parameters were directly optimized during simulation. In the case of spectra recorded at 298.5 K, the mean-field potential decomposition coefficients were varied, and order parameters were determined according to eqn (11). It was shown in ref. 41 that in this case the obtained order parameters can no longer be considered mutually independent. For this reason, determination of uncertainties of obtained order parameters and choosing the right truncation for the series of potential decomposition poses difficulties.

One can see that the order parameters determined for the supercooled smectic state at 100 K are higher than those determined for the smectic state at 298.5 K. This may originate from the structural changes, which take place during the cooling process. At lower temperatures the probe molecules may take more energetically favourable positions within the liquid crystalline matrix. Also, the high temperature spectra indicate

the presence of small biaxiality of the probe orientation $\left(\text{non-zero } \langle \mathbf{D}_{0,2}^{2*} \rangle \right)$.

Apart from the values of order parameters characterizing the degree of orientation order for the probe molecules, numerical simulation of the angular dependencies presented in Fig. 6 gives some additional information concerning the orientation of the spin probe. This information includes the direction of the orientation axis of the probe, i.e. the molecular axis, which is characterized by the largest degree of ordering.[14,49] The Euler angles, obtained from the EPR spectra, are listed in Table 2. For elongated molecules, such as the biradical used in the present work, one can expect that the orientation axis should be close to the longest molecular axis (smallest inertia axis). Contrary to this expectation, it has been found for the biradical probe used in this work that the orientation axis differs substantially from the long molecular axis. This is illustrated in Fig. 7. In this figure the green arrow indicates the direction of orientation principal axis, determined from the angular dependence of the supercooled smectic sample. The red arrow shows the principal axis of orientation determined from the EPR spectra recorded at 298.5 K, which coincides with the principal axis of the mean-field potential. It is seen that the orientation axis at both temperatures is close, and in both cases it is close to the y-axis of the nitroxide $\mathbf{g}$-tensor. The Euler angles $\mathbf{\Omega}_{g\to ori}$, which convert the $\mathbf{g}$-tensor into the orientation reference frame, are listed in Table 2 as well. One can see that they coincide within the experimental errors.

It should be noted that the possibility to reliably determine the orientation axes illustrates the advantage of using biradical spin probes. For nitroxide molecules, the nitrogen hyperfine splitting constant is almost axial. For this reason, for mono-radicals, it may be difficult to reliably discern between probe orientation along x- and y-axes of the nitroxide fragment. However, in the biradical reported in the present work, due to
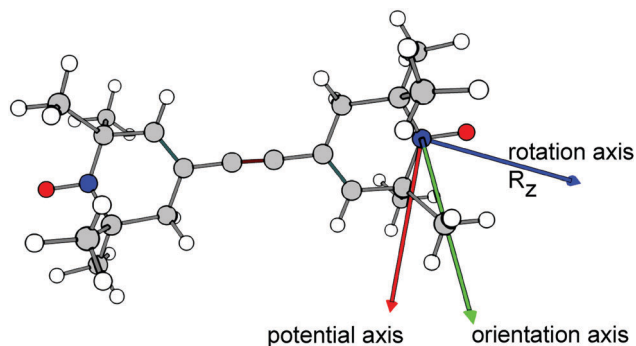
Fig. 7 Direction of principal axes of orientation (green arrow), mean-field potential (red arrow) and rotation diffusion (blue arrow) of the structure of the biradical probe.

the additional strongly anisotropic dipolar interaction directed along the x-axis of the probe, the x- and y-orientations are easily discerned.

Thus, the experimental data indicate that the molecules of the investigated biradical are preferentially ordered in both smectic and supercooled smectic 8CB in such a way that the liquid crystal director is aligned close to the y-axes of nitroxide moieties. This presents an unusual example of situation, in which an elongated molecule in liquid-crystalline media is aligned contrary to its geometrical shape. To rationalize this, one should keep in mind that the mode of orientation of admixture molecules in liquid crystals is determined by numerous factors, such as complexation, specific interactions, packing, and geometrical shape, and may not always be exclusively controlled by the latter factor.

The EPR spectra recorded at 298.5 K contain information about the probe rotations. The principal values of the rotation diffusion tensor are listed in Table 2. One important thing to note is the direction of the principal axis of rotation diffusion, shown in Fig. 7 defined by Euler angles $\Omega_{\text{Diff}\rightarrow\text{ori}}$, which convert the rotation diffusion tensor into the orientation reference frame. Whereas the principal orientation axis of the probe is directed close to the y-axis of the nitroxide moiety, the principal axis of rotation is directed close to the smallest inertia axis of the biradical. This reflects the fact that the fastest rotation takes place around the longest molecular axis of the probe.

Thus, in the case of the studied biradical in liquid crystalline 8CB, the principal axes of rotation and orientation are not the same. The physical meaning of such situation is the following. Although the turns along the elongated molecular axis are facilitated, the rotation is not uniform, *i.e.* during the rotation diffusion process the probe molecule spends more time with its y-axis aligned parallel to the liquid crystal director.

It should be noted that although the axis of the fastest rotation of the probe is close to the elongated molecular axis (x-axis of **g**-tensor), they do not coincide. The angle between these two axes is $(26 \pm 15)°$. It means that rotation diffusion of an admixture molecule inside the liquid-crystalline matrix is a complex process that involves both the movements and relative reorientations of the probe and the surrounding molecules,

and therefore is not solely defined by the probe geometry, but rather by the structures of transient complexes between the molecules of the probe and the matrix.

VIII. Conclusions

Quantitative numerical simulation of EPR spectra of the nitroxide biradical in two model systems has been accomplished in the present work. For the solution of the biradical in a viscous solvent (squalane), the temperature dependence of EPR spectra was analyzed, and two principal models of rotation mobility were used to account for spectral changes at different temperatures. Quasi-librations manifest themselves in the glassy state of the matrix, where the molecular rotation is restricted. At higher temperatures, the model of rotation diffusion is applicable for spectral simulation. Conformational dynamics was found to be reflected in the shape of EPR spectra (a) in the temperature dependence of the spin exchange constant and (b) in apparent axiality of the rotation diffusion tensor at temperatures higher than 284 K. Simulation of EPR spectra in the slow-motional regime allows determining the absolute sign of the spin exchange constant.

The numerical analysis of angular dependencies of EPR spectra of the biradical in the ordered liquid crystal (8CB) was used to obtain information about orientation alignment of the probe. The unusual mode of the probe orientation with respect to the liquid crystal director was discovered, and it has been shown that for the studied system the principal axes of orientation and rotation differ strongly.

We should note the consistency of the obtained results from the point of view of biradical magnetic parameters. All EPR spectra in this work, recorded at temperatures from 100 K to 370 K, both in isotropic and ordered samples, were simulated with the use of the single set of magnetic parameters, which supports the reliability of the measured characteristics of rotation and alignment.

References

1 *Advanced ESR Methods in Polymer Research*, ed. S. Schlick, Wiley-interscience, Hoboken, 2006.
2 D. A. Chernova and A. K. Vorobiev, *J. Appl. Polym. Sci.*, 2011, **121**, 102–110.

3 A. Bogdanov and A. Vorobiev, *J. Phys. Chem. B*, 2013, **117**, 12328–12338.

4 W. G. Miller, in *Spin Labeling: Theory and Applications*, ed. L. J. Berliner, Academic Press, New York, 1979, vol. 2, ch. 4, pp. 173–221.

5 S. A. Dzuba, *Spectrochim. Acta, Part A*, 2000, **56**, 227–234.

6 J. I. Spielberg and E. Gelerinter, *Phys. Rev. B: Condens. Matter Mater. Phys.*, 1984, **30**, 2319–2333.

7 G. R. Luckhurst and R. N. Yeates, *J. Chem. Soc., Faraday Trans. 2*, 1976, **72**, 996–1009.

8 C. F. Polnaszek and J. H. Freed, *J. Phys. Chem.*, 1975, **79**, 2283–2306.

9 C. Barcchiocchi, I. Miglioli, A. Arcioni, I. Vecchi, K. Rai, A. Fontecchio and C. Zannoni, *J. Phys. Chem. B*, 2009, **113**, 5391–5402.

10 T. S. Yankova, N. A. Chumakova, D. A. Pomogailo and A. K. Vorobiev, *Liq. Cryst.*, 2013, 1–11, DOI: 10.1080/02678292.2013.795621.

11 Z. Zhang, M. R. Fleissner, D. S. Tipikin, Z. Liang, J. K. Moscicki, K. A. Earle, W. L. Hubbell and J. H. Freed, *J. Phys. Chem. B*, 2010, **114**, 5503–5521.

12 K. Möbius and A. Savitsky, *High-field EPR Spectroscopy on Proteins and their Model Systems. Characterization of Transient Paramagnetic States.*, RSC Publishing, Cambridge, 2009.

13 *Biological Magnetic Resonance*, ed. L. J. Berliner, Spin Labeling The Next Millennium, Kluwer, 2002, vol. 14.

14 A. K. Vorobiev and N. A. Chumakova, in *Nitroxides – Theory, Experiment and Applications*, ed. A. I. Kokorin, InTech, Rijeka, 2012, ch. 3, pp. 57–112, DOI: 10.5772/74052.

15 D. E. Budil, S. Lee, S. Saxena and J. H. Freed, *J. Magn. Reson., Ser. A*, 1996, **120**, 155–189.

16 D. J. Schneider and J. H. Freed, in *Biological Magnetic Resonance, v. 8, Spin Labeling. Theory and Applications*, ed. L. J. Berliner, 1989, ch. 1, pp. 1–76.

17 V. Barone and A. Polimeno, *Phys. Chem. Chem. Phys.*, 2006, **8**, 4609–4629.

18 S. Stoll and A. Schweiger, *J. Magn. Reson.*, 2006, **178**, 42–55.

19 G. R. Luckhurst, in *Spin Labeling, Theory and Application*, ed. L. J. Berliner, Academic, New York, 1976, pp. 133–181.

20 G. R. Luckhurst and G. F. Pedulli, *Mol. Phys.*, 1970, **18**, 425–428.

21 V. N. Parmon and G. M. Zhidomirov, *Mol. Phys.*, 1974, **27**, 367–375.

22 V. N. Parmon, A. I. Kokorin, G. M. Zhidomirov and K. I. Zamaraev, *Mol. Phys.*, 1975, **30**, 695–701.

23 G. R. Luckhurst and G. F. Pedulli, *Mol. Phys.*, 1971, **20**, 1043–1055.

24 G. R. Luckhurst, R. Poupko and C. Zannoni, *Mol. Phys.*, 1975, **30**, 499–515.

25 A. Polimeno, M. Zerbetto, L. Franco, M. Maggini and C. Covaja, *J. Am. Chem. Soc.*, 2006, **128**, 4734.

26 T. Kálai, J. Jekő, Z. Berente and K. Hideg, *Synthesis*, 2006, 439.

27 A. J. Leadbetter, J. L. A. Durrant and M. Rugman, *Mol. Cryst. Liq. Cryst.*, 1976, **34**, 231–235.

28 K. Negita, *Mol. Cryst. Liq. Cryst.*, 1997, **300**, 163–178.

29 R. J. Ondris-Crawford, G. P. Crawford, J. W. Doane, S. Žumer, M. Vilfan and I. Vilfan, *Phys. Rev. E: Stat. Phys., Plasmas, Fluids, Relat. Interdiscip. Top.*, 1993, **48**, 1998–2005.

30 A. Schweiger and G. Jeschke, *Principles of Pulse Electron Paramagnetic Resonance*, Oxford University Press, New York, 2001.

31 S. M. Blinder, *J. Chem. Phys.*, 1960, **33**, 748.

32 V. N. Parmon, A. I. Kokorin and G. M. Zhidomirov, *Stable biradicals (in Russian)*, Nauka, Moscow, 1980.

33 J. Charles P. Poole and P. Poole, *Electron Spin Resonance. A Comprehensive Treatise on Experimental Techniques*, Interscience, New York, 1967.

34 C. Zannoni, in *The Molecular Physics of Liquid Crystals*, ed. G. R. Luckhurst and G. W. Gray, Academic Press, 1979, ch. 3, pp. 51–83.

35 R. Kubo, *Adv. Chem. Phys.*, 1969, **15**, 101–127.

36 C. F. Polnaszek, G. V. Bruno and J. H. Freed, *J. Chem. Phys.*, 1973, **58**, 3185–3199.

37 J. H. Freed, in *Spin labeling. Theory and applications*, ed. L. J. Berliner, Academic Press, London, 1976, ch. 3, pp. 53–132.

38 E. Meirovitch, D. Inger, E. Inger, G. Moro and J. H. Freed, *J. Chem. Phys.*, 1982, **77**, 3915.

39 K. V. Vasavada, D. J. Schneider and J. H. Freed, *J. Chem. Phys.*, 1987, **86**, 647.

40 R. Tarroni and C. Zannoni, *J. Chem. Phys.*, 1991, **95**, 4550–4564.

41 A. K. Vorobiev, T. S. Yankova and N. A. Chumakova, *Chem. Phys.*, 2012, **409**, 61–73.

42 J. E. Dennis, D. M. Gay and R. E. Welsch, *ACM Transactions on Mathematical Software*, 1981, **8**, 348–368.

43 S.-y. Kishioka, T. Ohsaka and K. Tokuda, *Electrochim. Acta*, 2003, **48**, 1589–1594.

44 D. A. Chernova and A. K. H. Vorobiev, *J. Polym. Sci., Part B: Polym. Phys.*, 2009, **47**, 107–120.

45 A. V. Bogdanov and A. K. Vorobiev, *Chem. Phys. Lett.*, 2011, **506**, 46–51.

46 O. I. Gromov, E. N. Golubeva, V. N. Khrustalev, T. Kálai, K. Hideg and A. I. Kokorin, *Appl. Magn. Reson.*, 2014, **45**, 981–992.

47 H. Eyring, *J. Chem. Phys.*, 1935, **3**, 107.

48 A. L. Buchachenko and A. M. Wasserman, *Stable Radicals. Electronic structure, reactivity and applications (in Russian)*, Khimiya, Moscow, 1973.

49 S. G. Carr, S. K. Khoo, G. R. Luckhurst and C. Zannoni, *Mol. Cryst. Liq. Cryst.*, 1976, **35**, 7–13.